

DTIC FILE COPY

Naval Research Laboratory

Washington, DC 20375-5000

(2)



NRL Report 9273

AD-A226 616

Missing Pulse Clutter Processing

MICHAEL STEINER AND FRANK F. KRETSCHMER, JR.

*Target Characteristics Branch
Radar Division*

DTIC
ELECTE
SEP 17 1990
S D CS D

August 31, 1990


Approved for public release; distribution unlimited.

90 09 11 131

| REPORT DOCUMENTATION PAGE | | | Form Approved OMB No. 0704-0188 | |
|--|---|--|---------------------------------------|--|
| Public reporting burden for this collection of information is estimated to average 1 hour per response, including the time for reviewing instructions, searching existing data sources, gathering and maintaining the data needed, and completing and reviewing the collection of information. Send comments regarding this burden estimate or any other aspect of this collection of information, including suggestions for reducing this burden, to Washington Headquarters Services, Directorate for Information Operations and Reports, 1215 Jefferson Davis Highway, Suite 1204, Arlington, VA 22202-4302, and to the Office of Management and Budget, Paperwork Reduction Project (0704-0188), Washington, DC 20503. | | | | |
| 1. AGENCY USE ONLY (Leave blank) | 2. REPORT DATE August 31, 1990 | 3. REPORT TYPE AND DATES COVERED Interim | | |
| 4. TITLE AND SUBTITLE Missing Pulse Clutter Processing | | 5. FUNDING NUMBERS PE - 62111N TA - TARA11-P10-OPO WU - DN159-039 | | |
| 6. AUTHOR(S) Michael J. Steiner and Frank F. Kretschmer, Jr. | | | | |
| 7. PERFORMING ORGANIZATION NAME(S) AND ADDRESS(ES) Naval Research Laboratory Washington, DC 20375-5000 | | 8. PERFORMING ORGANIZATION REPORT NUMBER NRL Report 9273 | | |
| 9. SPONSORING / MONITORING AGENCY NAME(S) AND ADDRESS(ES) Office of Naval Research Office of Naval Technology Arlington, VA 22217 | | 10. SPONSORING / MONITORING AGENCY REPORT NUMBER | | |
| 11. SUPPLEMENTARY NOTES | | | | |
| 12a. DISTRIBUTION / AVAILABILITY STATEMENT Approved for public release; distribution unlimited. | | | 12b. DISTRIBUTION CODE | |
| 13. ABSTRACT (Maximum 200 words) Missing pulses resulting from RFI blanking, ambiguous range returns when no filler pulses are used, or eclipsing can seriously degrade conventional clutter filters. This report investigates the effects of a missing pulse on uncompensated and optimum clutter filters. The maximum improvement factor method of Emerson and other methods are compared to the optimum filtering. New methods and results using a minimax log energy search method are described and are shown to provide performance and/or implementation complexity advantages. | | | | |
| 14. SUBJECT TERMS Interference Matched filtering Clutter processing | | | 15. NUMBER OF PAGES 23 | |
| 16. PRICE CODE | | | | |
| 17. SECURITY CLASSIFICATION OF REPORT UNCLASSIFIED | 18. SECURITY CLASSIFICATION OF THIS PAGE UNCLASSIFIED | 19. SECURITY CLASSIFICATION OF ABSTRACT UNCLASSIFIED | 20. LIMITATION OF ABSTRACT SAR | |

CONTENTS

| | |
|---|----|
| 1. INTRODUCTION | 1 |
| 2. PERFORMANCE DEGRADATION BY USING CONVENTIONAL CLUTTER FILTERS | 1 |
| 3. OPTIMAL FILTER PERFORMANCE | 3 |
| 4. SINGLE AND MULTIPLE FILTER WEIGHTING TECHNIQUES | 13 |
| 5. IMPLEMENTATION | 17 |
| 6. SUMMARY | 18 |
| 7. REFERENCES | 18 |



| | |
|--------------------|--------------------|
| Accession No. | |
| DTIC Class. | ✓ |
| DTIC Type | [] |
| Unannounced | [] |
| Justified | |
| By _____ | |
| Distribution/ | |
| Availability Codes | |
| Dist | Availability Codes |
| A-1 | |

MISSING PULSE CLUTTER PROCESSING

1. INTRODUCTION

Missing radar return pulses in a coherent processing interval (CPI) can seriously degrade the clutter processing and detection performance of a radar. The clutter processing is degraded by missing pulses for either a moving target indication (MTI) filter or a Doppler filter bank. Missing pulses can occur for several different reasons. Missing pulses result from the blanking of strong interference pulses that may be received from an emitter. These pulses are usually blanked to avoid the associated false alarms or to avoid desensitizing a radar that is using constant false alarm rate (CFAR) processing. Missing pulses can occur in the returns from ambiguous range intervals if no filler pulses are used. They can also occur in radar return pulses that are eclipsed by transmissions that occur at the same time as the return pulse. By proper design, new filter weights can substantially reduce losses resulting from a missing pulse. In this report we consider a single missing pulse in a CPI consisting of N pulses. New weighting techniques are investigated, and the results of Ref. 1 are extended to describe the losses that occur relative to the no-missing-pulse case for nonoptimal and optimal processing (optimal is in the Neyman-Pearson sense).

Section 2 examines the performance of conventional clutter processing techniques when a missing pulse occurs. Section 3 presents optimal processing for the missing pulse case. Results are given that show the effects of missing pulses relating to the number of pulses in a CPI, the normalized spectral width of the clutter power spectrum, and the clutter-to-thermal-noise ratio. Section 4 provides techniques for finding suboptimum filters that trade off processing complexity. Section 5 considers implementations of these designs.

2. PERFORMANCE DEGRADATION BY USING CONVENTIONAL CLUTTER FILTERS

When a pulse is missing, the performance of a filter degrades relative to the no-missing-pulse case. This degradation in the ability to cancel clutter is examined when conventional filters are used.

We first illustrate the degradation for a conventional four-pulse MTI filter that incorporates a binomial weighting of $(1, -3, 3, -1)$ for the no-missing-pulse case P_0 . The i th missing-pulse case is designated by P_i , and the effective performance can be obtained by zeroing the i th weighting coefficient of the filter. Thus, for the four-pulse MTI, P_1 corresponds to a filter weighting of $(0, -3, 3, -1)$. Figure 1(a) shows the transfer function $10 \log |H(f)|^2$ for the four-pulse canceller plotted on the normalized frequency scale f , where f is the ratio of the Doppler frequency f_d to the pulse repetition frequency f_r . $H(f)$ is the Fourier transform of the impulse response of the four-pulse canceller. Figures 1(b) and 1(c) show the transfer functions for missing first and second pulses, respectively. The power spectral density of the filtered clutter is given by the product of the power spectral density of the clutter and $|H(f)|^2$. From these figures, it is apparent that cancellation of clutter having a Gaussian power spectrum centered at zero frequency is seriously degraded by the large sidelobes of the transfer functions for the missing-pulse cases.

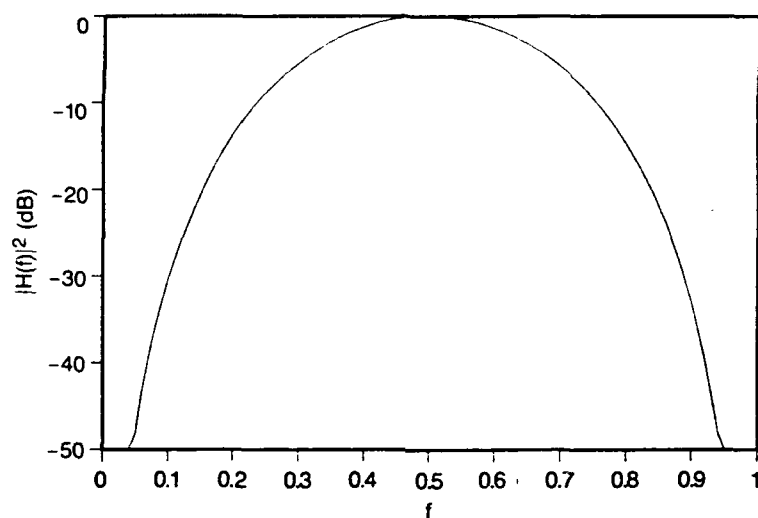


Fig. 1(a) — $|H(f)|^2$ vs f , $N = 4$, P_0

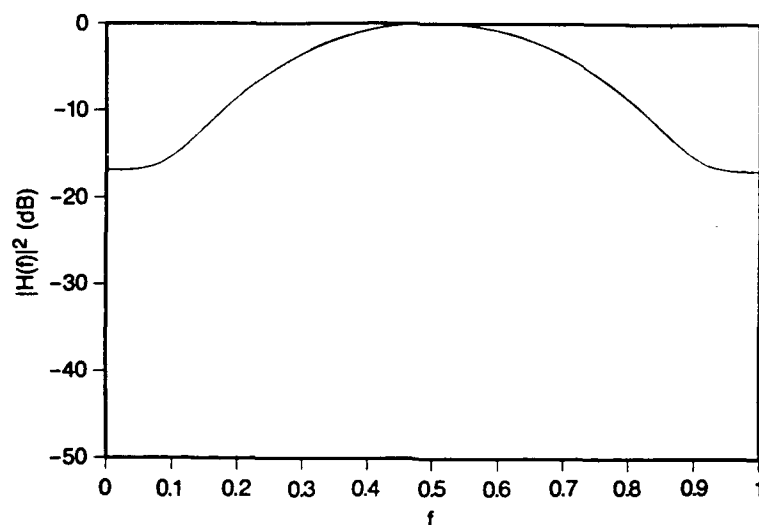


Fig. 1(b) — $|H(f)|^2$ vs f , $N = 4$, P_1

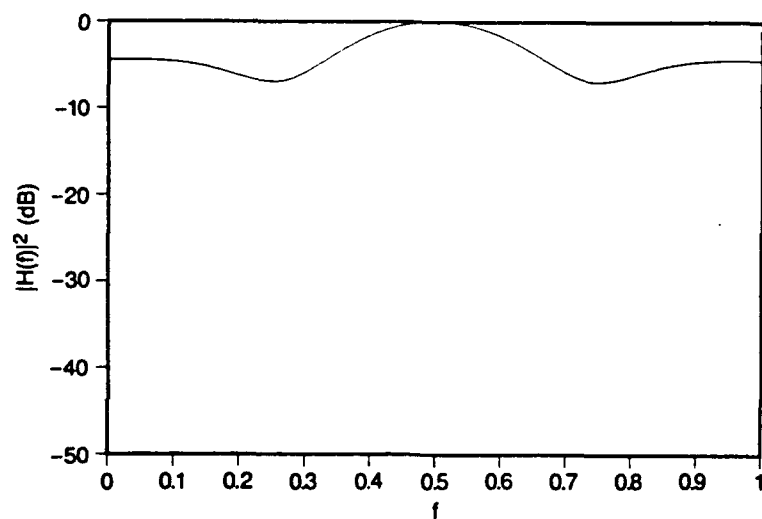


Fig. 1(c) — $|H(f)|^2$ vs f , $N = 4$, P_2

Figures 2 and 3 show a similar degradation in the ability to cancel clutter. Figure 2(a) shows the transfer function of the center filter of an eight-point, unweighted Doppler filter bank with no missing pulse. Figures 2(b) and 2(c) show the degradation in the sidelobes for missing first and fourth pulses, respectively. Figure 3 shows similar plots for the center filter of an eight-pulse Chebychev filter bank designed with -40 dB sidelobes. Figures 1 to 3 show that the ability to cancel clutter diminishes as the missing pulse location becomes closer to the middle of the pulse train. These results are similar to those of Ward [2], who showed the degradation caused by missing end pulses that result from ambiguous range returns.

3. OPTIMAL FILTER PERFORMANCE

We next describe the effects of missing pulses for filters that have a weight vector w_0 that maximizes the probability of detection for a fixed probability of false alarm in Gaussian interference. The interference consists of clutter plus thermal noise. w_0 , in Gaussian interference, is also the vector that maximizes the signal-to-interference ratio S/I . The optimal vector w_0 is well known and is given by

$$w_0 = kR^{-1}S^*, \quad (1)$$

where R denotes the $N \times N$ covariance matrix of interference, which in turn is given by

$$E(X^*X'), \quad (2)$$

where X is an $N \times 1$ vector denoting the N interference returns, $*$ denotes conjugation, and $'$ denotes transpose. k is a nonzero complex constant. Note in general that the weight w is complex. In Eq. (1), S is an $N \times 1$ vector representing the moving target signal given by

$$S = \begin{pmatrix} e^{j\psi} \\ e^{j2\psi} \\ \vdots \\ e^{jN\psi} \end{pmatrix}, \quad (3)$$

where $\psi = 2\pi f$. First, an N -pulse single filter is described that is matched to a single Doppler frequency. Figure 4(a) shows the transfer function for a five-pulse filter matched to a target whose normalized Doppler shift is $f = 0.5$, and for a normalized spectral width $\sigma T = .05$, where σ is the standard deviation of the Gaussian power spectrum and T is the interpulse interval that is equal to $1/f_r$. The clutter-to-thermal-noise ratio C/N_0 is equal to 30 dB, and the clutter spectrum is centered at zero frequency. Figure 4(b) shows the transfer function for the third pulse missing. The new weighting is found by zeroing the third row and column of R and the third element of S in Eq. (1). Again, the increase in the sidelobe level in the region of the clutter as seen in Figs. 4(a) and 4(b) for the optimized single filters.

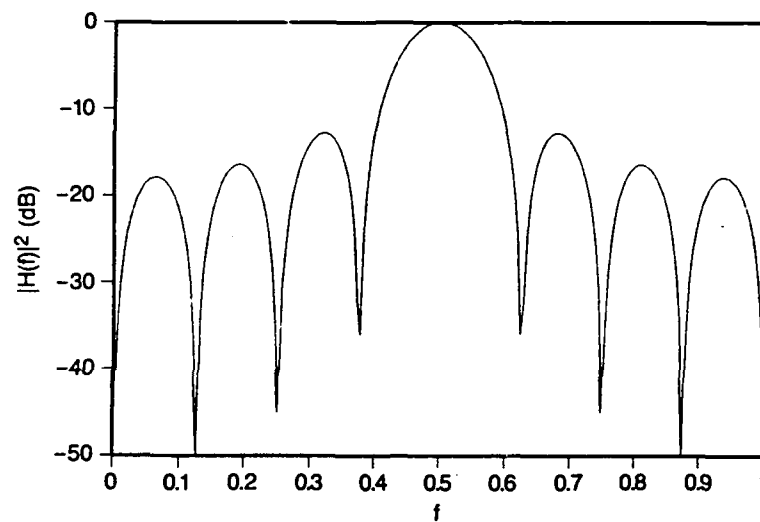


Fig. 2(a) — $|H(f)|^2$ vs f , $N = 8$, P_0 , uniform weighting

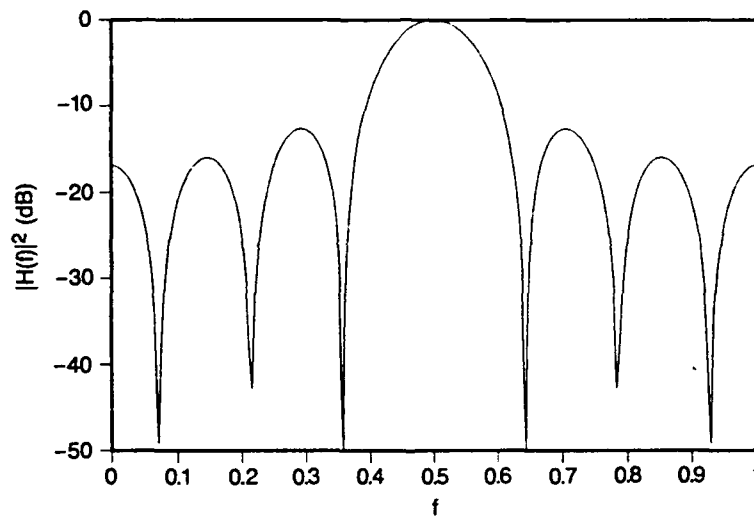


Fig. 2(b) — $|H(f)|^2$ vs f , $N = 8$, P_1 , uniform weighting

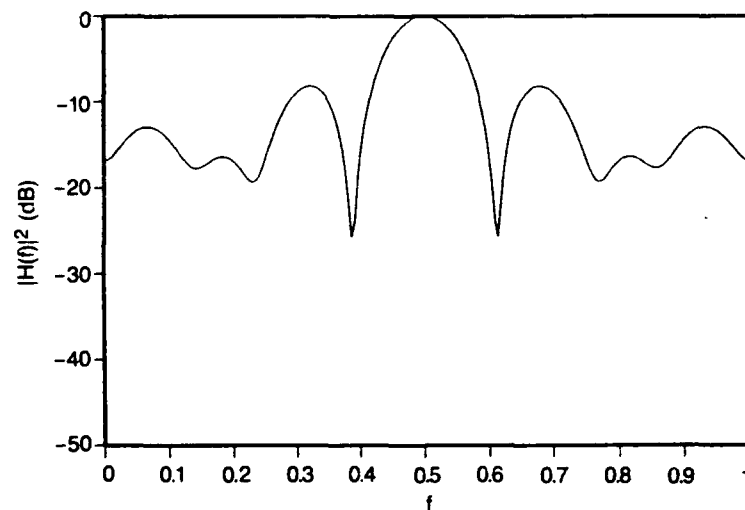


Fig. 2(c) — $|H(f)|^2$ vs f , $N = 8$, P_4 , uniform weighting

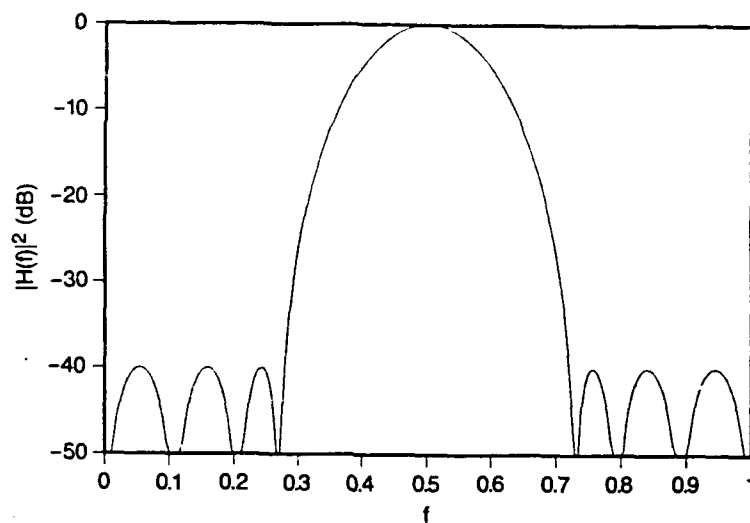


Fig. 3(a) — $|H(f)|^2$ vs f , $N = 8$, P_0 , Chebychev weighting

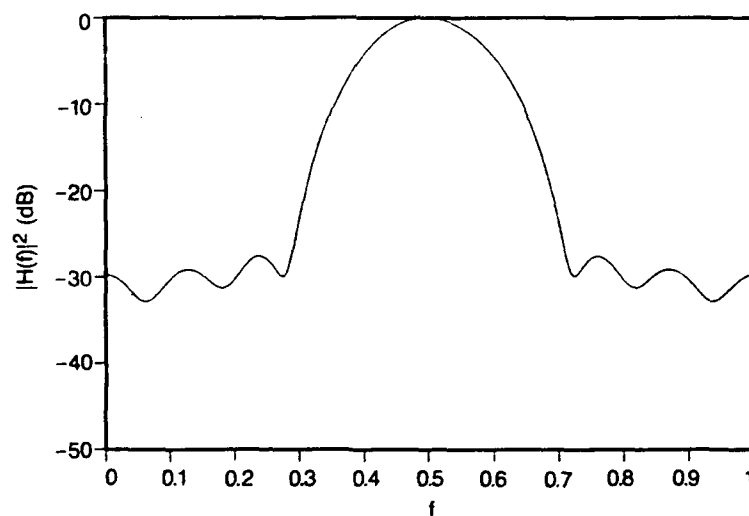


Fig. 3(b) — $|H(f)|^2$ vs f , $N = 8$, P_1 , Chebychev weighting

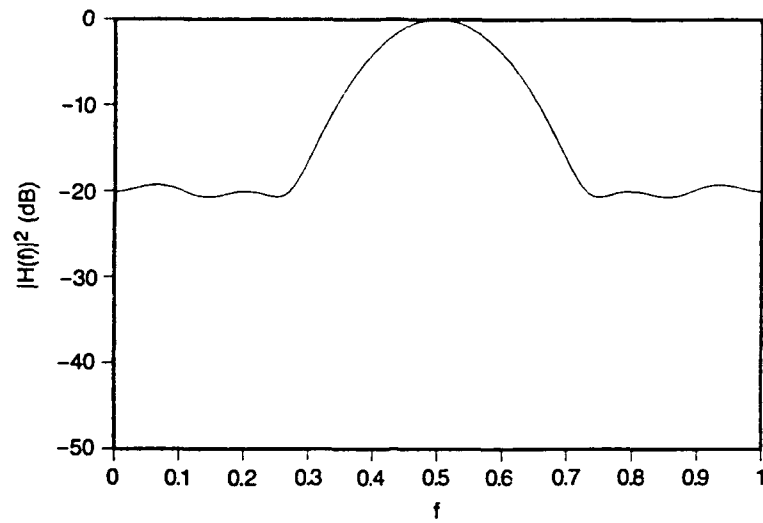


Fig. 3(c) — $|H(f)|^2$ vs f , $N = 8$, P_2 , Chebychev weighting

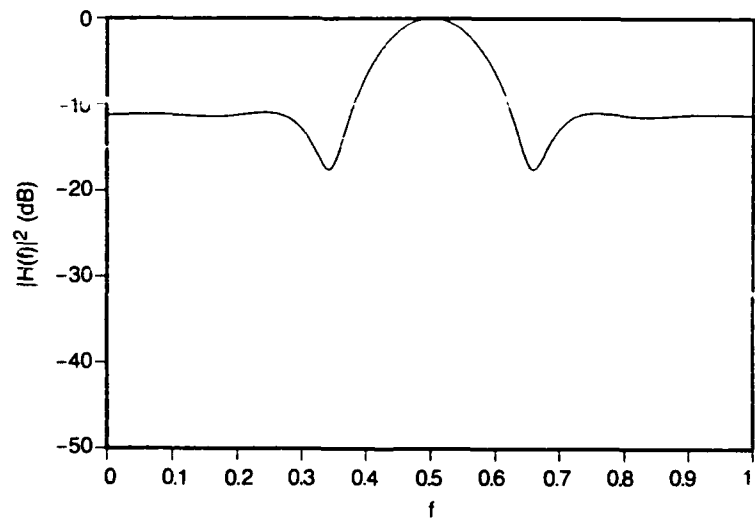


Fig. 3(d) — $|H(f)|^2$ vs f , $N = 8$, P_4 , Chebychev weighting

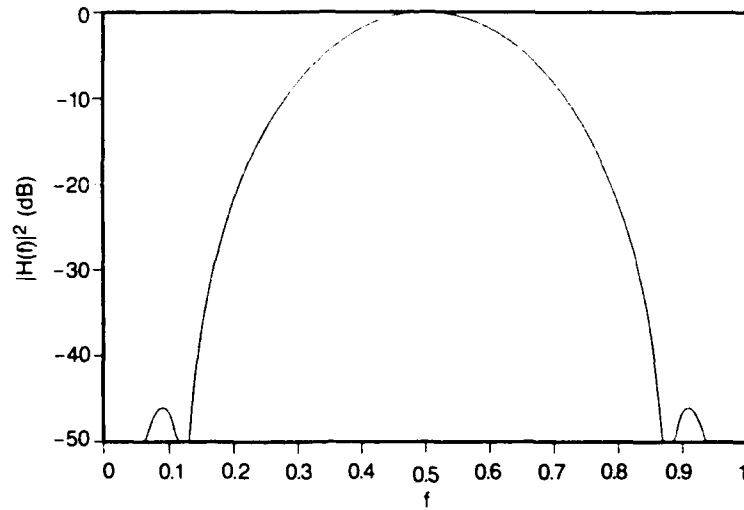


Fig. 4(a) — $|H(f)|^2$ vs f , $N = 5$, P_0 , $C/N_0 = 30$ dB, $\sigma T = 0.05$

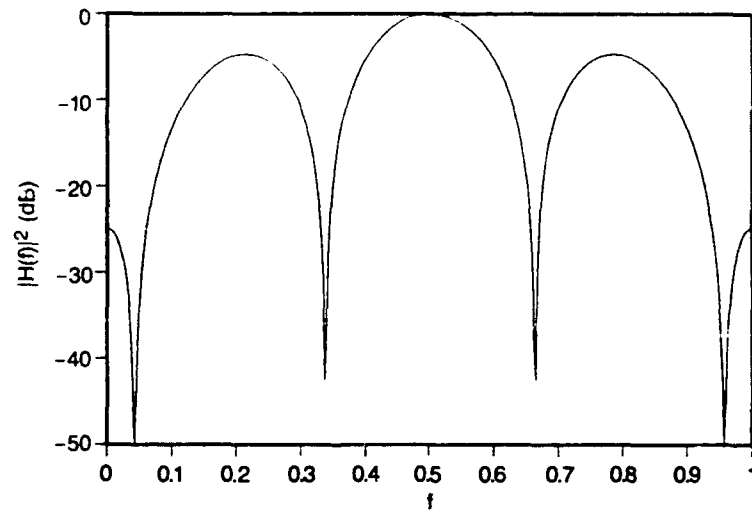


Fig. 4(b) — $|H(f)|^2$ vs f , $N = 5$, P_3 , $C/N_0 = 30$ dB, $\sigma T = 0.05$

A measure used to assess the performance of a given filter is the gain or improvement of (S/I) as a function of frequency. The gain is defined as

$$(S/I)_o / (S/I)_i,$$

where $(S/I)_o$ is the signal-to-interference ratio out of the filter and $(S/I)_i$ is the signal-to-interference ratio into the filter. For a weighting vector, \mathbf{w} , the gain at the match point is then given by

$$G(f) = \frac{|\mathbf{w}'\mathbf{S}|^2}{\gamma \mathbf{w}'\mathbf{R}\mathbf{w}}, \quad (4)$$

where γ equals $(S/I)_i$ and \dagger denotes the conjugate transpose. The gain is maximized by using the matched filter weighting (Eq. (1)) at each frequency. Figure 5(a) shows the matched filter gain as a function of frequency for a four-pulse processor having an input C/N_0 of 50 and 10 dB. The solid curve corresponds to no missing pulse, and the curves designated by P_i correspond to the recomputed optimum gain curves for the i th missing pulse case. At each frequency, a different optimal filter, given by Eq. (1), is used that is matched to the corresponding frequency. Large differences between the optimal gain when no pulses are missing and the optimal gain when a pulse is missing can be seen in Fig. 5(a) for C/N_0 equal to 50 dB. This difference, which is a function of frequency, is termed loss. Figures 5(b)-5(d) show similar plots for increasing N . Note the large loss for the P_3 case at $f = 0.5$ in Fig. 5(b). For the larger number of pulses shown in Figs. 5(c) and 5(d), the losses diminish. Figure 6 shows the loss at $f = 0.5$ vs N for the centermost pulse missing, different C/N_0 ratios, and for $\sigma T = 0.05$. A threshold effect is noted, which shows a rapid decrease in the loss for values of N larger than the threshold values. In Fig. 7, the loss at $f = 0.5$ is plotted against σT for $N = 6$, with the third pulse missing and for different C/N_0 . Figure 8 shows the loss at $f = 0.5$ vs σT for different N , the centermost pulse missing, and for $C/N_0 = 30$ dB. These curves show that the loss decreases with decreasing C/N_0 and increasing N , and also that the loss is dependent on σT . Figure 9 shows the gain measured at $f = 0.5$ vs σT for $N = 6$, a missing third pulse, and for $C/N_0 = 10, 30$, and 50 dB. Note that although the losses shown in Fig. 7 peak, the actual gain curves monotonically increase as σT decreases. Figure 10 shows the gain measured at $f = 0.5$ vs σT for $N = 4, 8$, and 16, the centermost pulse missing, and $C/N_0 = 30$ dB. Again the gain monotonically increases as σT decreases. The loss curves indicate the actual losses that are incurred for the missing-pulse case relative to the no-missing-pulse case. In each situation, optimum weights are used. On the other hand, the gain curves of Figs. 9 and 10 show the maximum theoretical gains for the missing-pulse case. These curves are important from a system design standpoint. We mention, at this point, that usually the loss is greatest at $f = 0.5$ for a missing pulse near the center of the N pulses; however, computations have shown this is not always the case.

Figure 11 shows the degradation in the gain if the optimum weights for the no-missing-pulse case P_0 are used for the missing third pulse case. This curve is designated P_{03} . The P_3 curve shows the gain when the weights are optimized for the third pulse missing. The parameters for Fig. 11 are $N = 5$, $C/N_0 = 50$ dB, and $\sigma T = 0.05$.

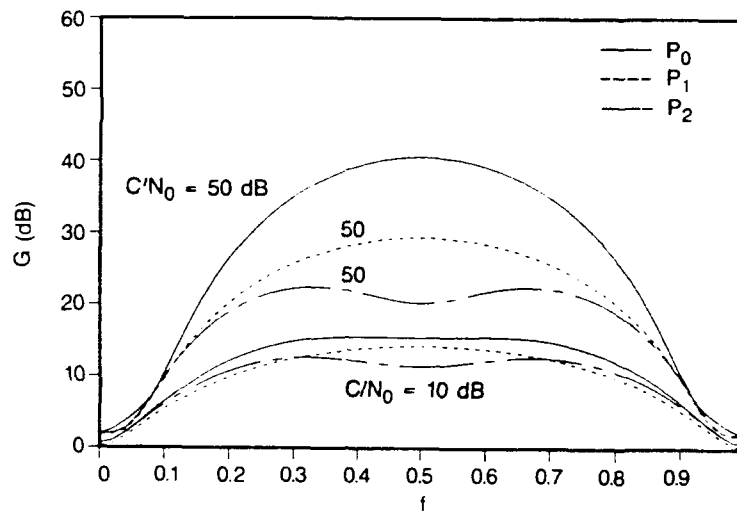


Fig. 5(a) — G vs f ; $N = 4$, optimum filters, $\sigma T = 0.05$

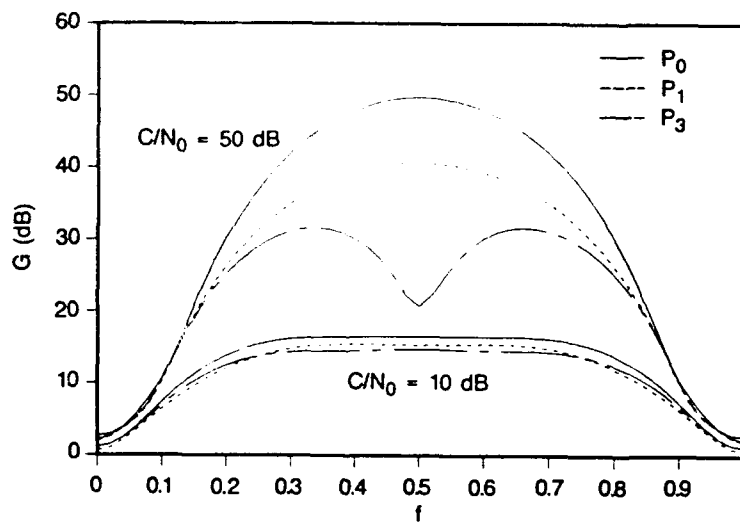


Fig. 5(b) — G vs f ; $N = 5$, optimum filters, $\sigma T = 0.05$

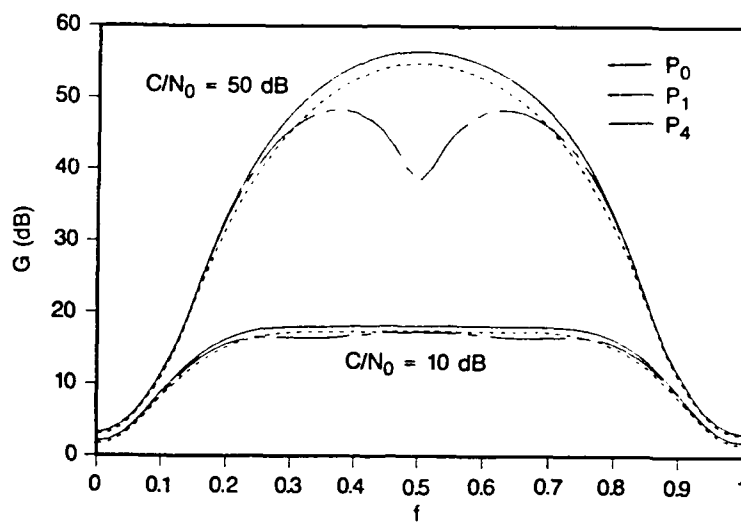


Fig. 5(c) — G vs f ; $N = 7$, optimum filters, $\sigma T = 0.05$

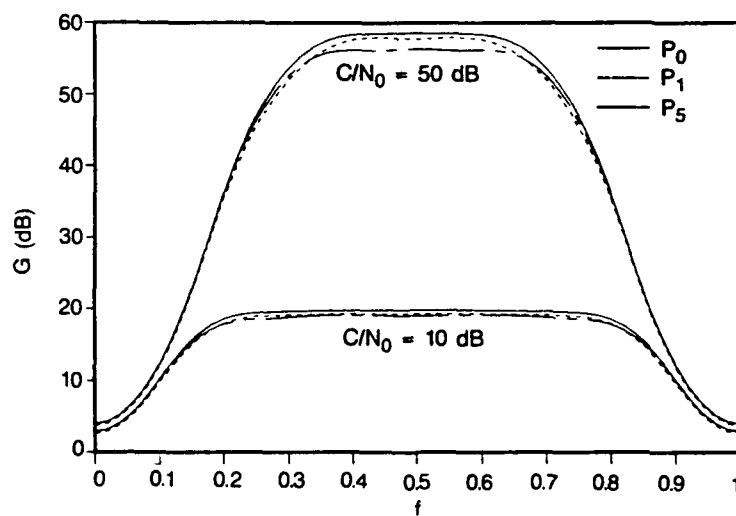


Fig. 5(d) — G vs f ; $N = 10$, optimum filters, $\sigma T = 0.05$

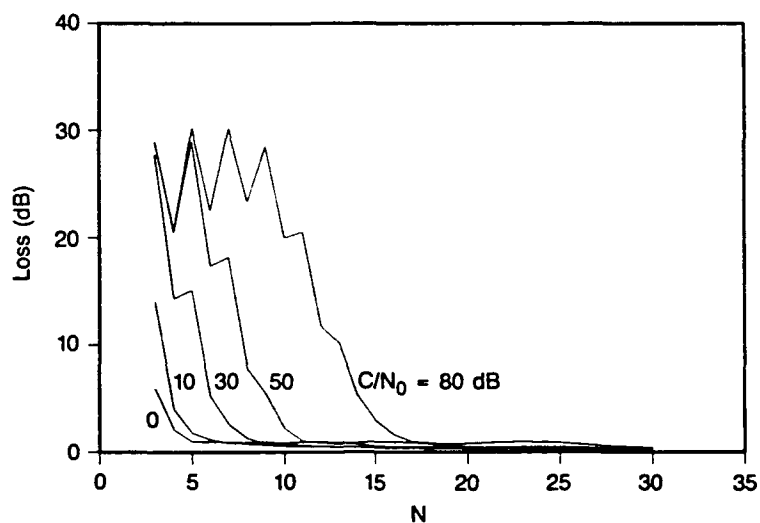


Fig. 6 — Loss vs N ; centermost pulse missing, $f = 0.5$, $\sigma T = 0.05$

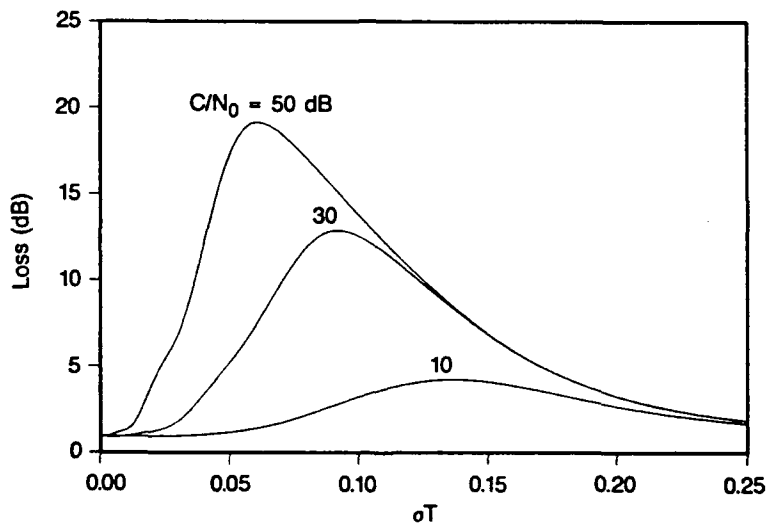


Fig. 7 — Loss vs σT , $N = 6$, P_3 , $f = 0.5$

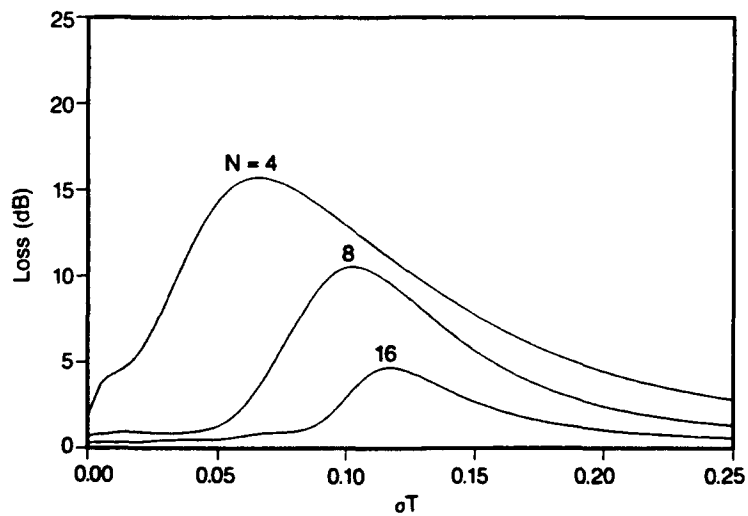


Fig. 8 — Loss vs σT , centermost pulse missing, $C/N_0 = 30 \text{ dB}$, $f = 0.5$

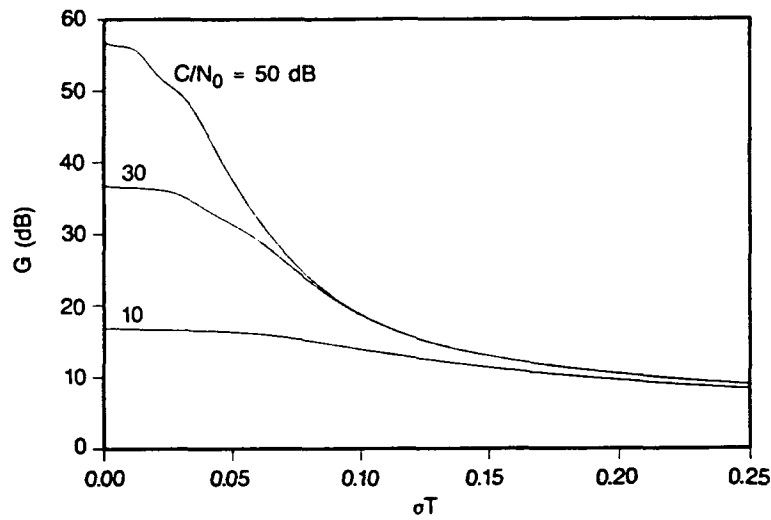


Fig. 9 — G vs σT , $N = 6$, P_3 , $f = 0.5$

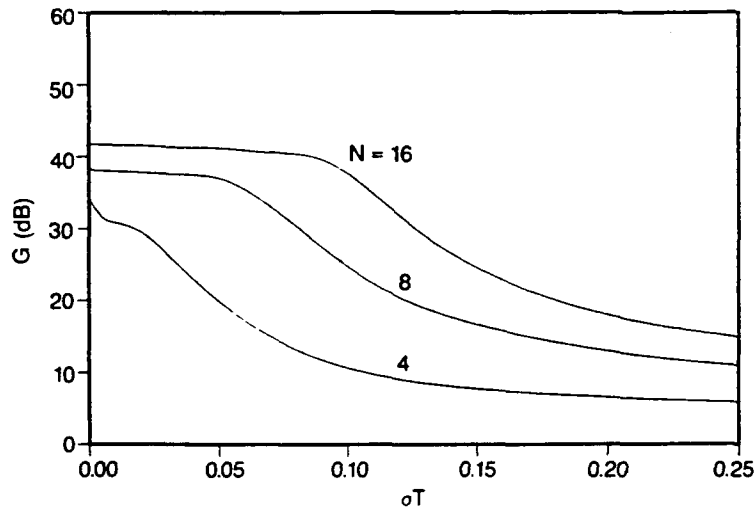


Fig. 10 — G vs σT , centermost pulse missing, $C/N_0 = 30$ dB, $f = 0.5$

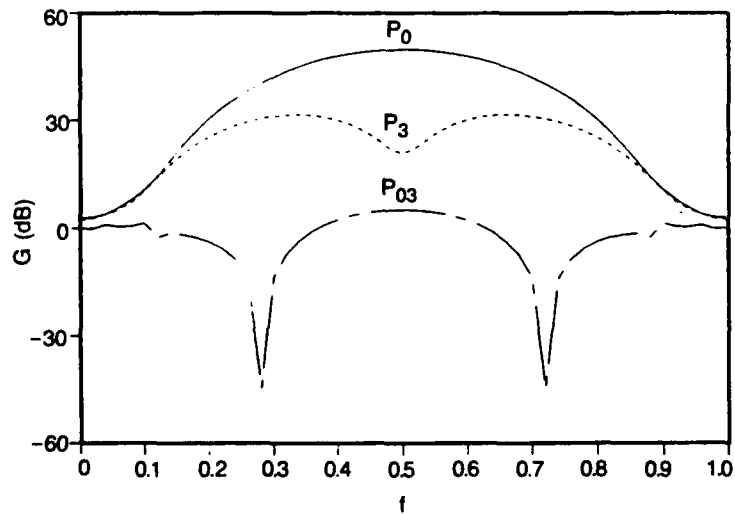


Fig. 11 — G vs f , $N = 5$, $C/N_0 = 50$ dB, $\sigma T = 0.05$

4. SINGLE AND MULTIPLE FILTER WEIGHTING TECHNIQUES

This section describes techniques for determining single and multiple filter characteristics that closely approximate the optimum filter performance described above for a given missing-pulse location. First, filter implementations are described for a single filter that spans the Doppler passband.

Reference 1 suggests a method whereby the matched filter weights found at several values of frequency are linearly combined by trial and error. The problem, in general, is that it may be difficult to determine the appropriate frequencies and combination of weightings. A design method for single filters due to Emerson [3] was investigated for the missing-pulse case. Here a weighting is sought that maximizes the improvement factor. The improvement factor is the average gain, where the averaging is done over frequency. This weighting is determined by the eigenvector corresponding to the minimum eigenvalue of the covariance matrix. A method of linearly combining eigenvectors of the covariance matrix due to Fletcher [4] was also investigated. We found that these eigenvector methods are not satisfactory in general for the missing-pulse case. A new method, to be described, was investigated that provides improved performance by using a minimax method implemented by means of a search algorithm.

It has been found, for the cases investigated, that using the eigenvector weighting corresponding to the minimum eigenvector results in poor performance when the center pulse is missing for N odd. Figure 12 shows the optimum gains of a five-pulse processor having no missing pulses and a missing center pulse, and the bottom curve corresponds to the Emerson eigenvector weighting associated with the minimum eigenvalue. A large loss in gain occurs around $f = 0.5$. A second eigenvector method, also from Ref. 4, was investigated where the weighting is given by

$$\mathbf{w} = e_{11}^* \mathbf{e}_1 + e_{21}^* \mathbf{e}_2 + \dots + e_{r1}^* \mathbf{e}_r, \quad r \leq N \quad (5)$$

where e_{j1} is the first element of the j th eigenvector. This weighting is derived in Ref. 4 to minimize the departure of the filter transfer function from a flat passband subject to the constraints that the filter weight is constrained to the space of the r eigenvectors of the covariance matrix. By combining more eigenvectors, the passband becomes flatter at the expense of a reduced average gain. However, this method did not work well for the missing-pulse case. Results are shown in Fig. 13 for $r = 2$. The second method in Ref. 4 of imposing an additional constraint on the improvement factor was not considered. Other eigenvector weightings have been investigated by the authors, and only in some cases were good results obtained.

A different method, which overcomes these difficulties and results in good performance, is the minimax log energy (MMLE) method [5]. Here a weighting \mathbf{w} is found by iteration, such that

$$\mathbf{w} \in \arg \min_w \max_f \{ \log G_{opt}(f) - \log G_w(f) \}, \quad (6)$$

where $G_{opt}(f)$ is the optimal gain function achievable by optimal filters (1) corresponding to f . $G_w(f)$ is the gain function for the single filter with weighting \mathbf{w} . This amounts to minimizing the maximum deviation between the log of the optimal gain and the log of the gain when the single weight \mathbf{w} is used. The frequency span over which this search takes place is prespecified. Figure 14 shows the results of applying this method for a single filter weighting.

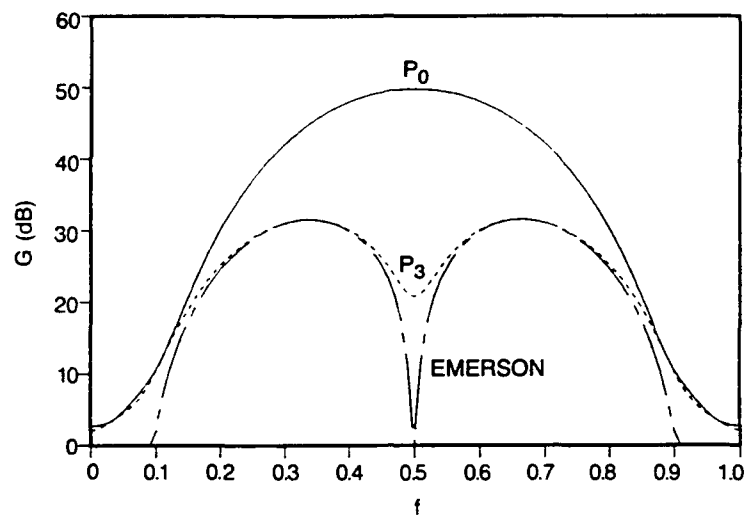


Fig. 12 — G vs f , $N = 5$, $C/N_0 = 50$ dB, $\sigma T = 0.05$

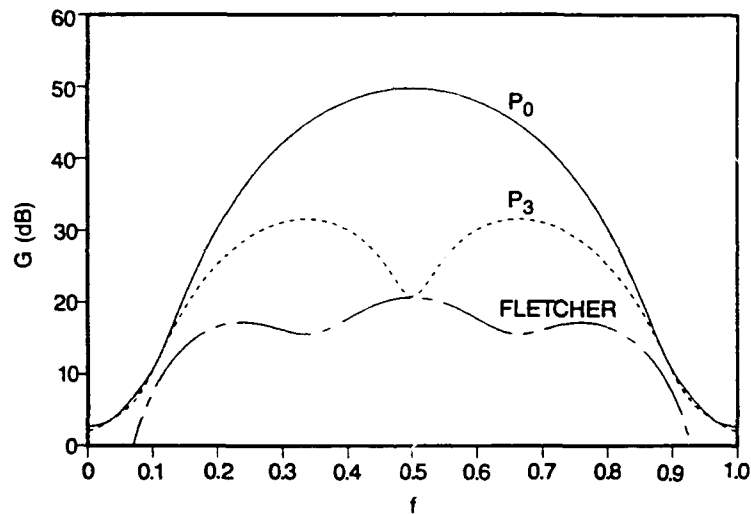


Fig. 13 — G vs f , $N = 5$, $C/N_0 = 50$ dB, $\sigma T = 0.05$

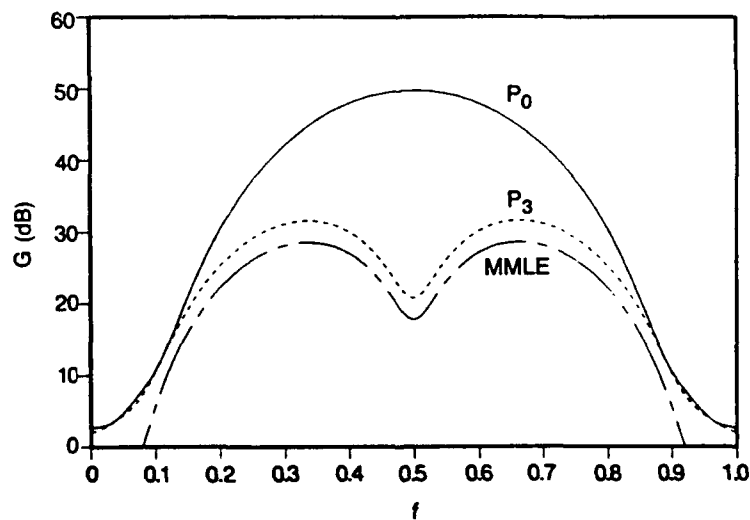


Fig. 14 — G vs f , $N = 5$, $C/N_0 = 50$ dB, $\sigma T = 0.05$

To derive multiple filters that approximate the optimum gain curves for a given missing-pulse location, it is found that the method of Andrews [6] can be incorporated to give a good approximation to the optimum gain curve. This method consists of maximizing the S/I improvement factor within each of the subbands of N -filters equally spaced across the Doppler space. In this formulation the signal Doppler is assumed to be uniformly distributed across each subband. Figure 15 shows the results of this design approach for $N = 8$, with no missing pulse and for pulse number 4 missing, respectively. These figures show the contour of the maximum gains of the eight filters, i.e., $G(f) = \max_i G_i(f)$, $i = 1, 2, \dots, 8$, where $G_i(f)$ is the gain function for the i th filter.

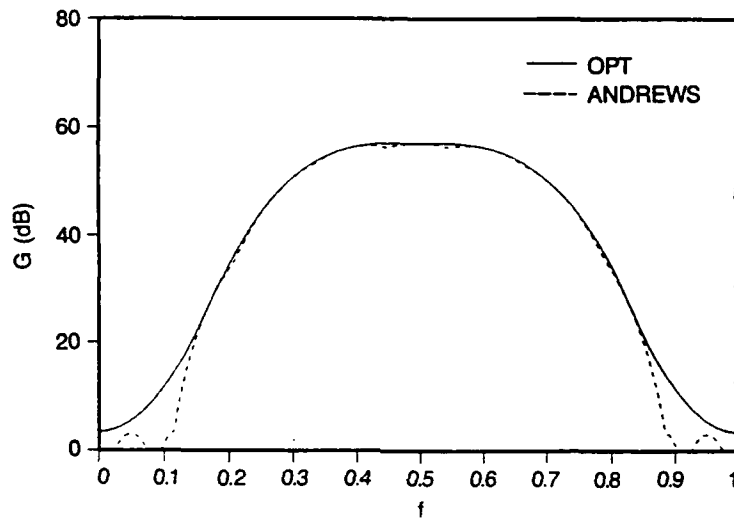


Fig. 15(a) — G vs f , $N = 8$, P_0 , $C/N_0 = 50$ dB, $\sigma T = 0.05$

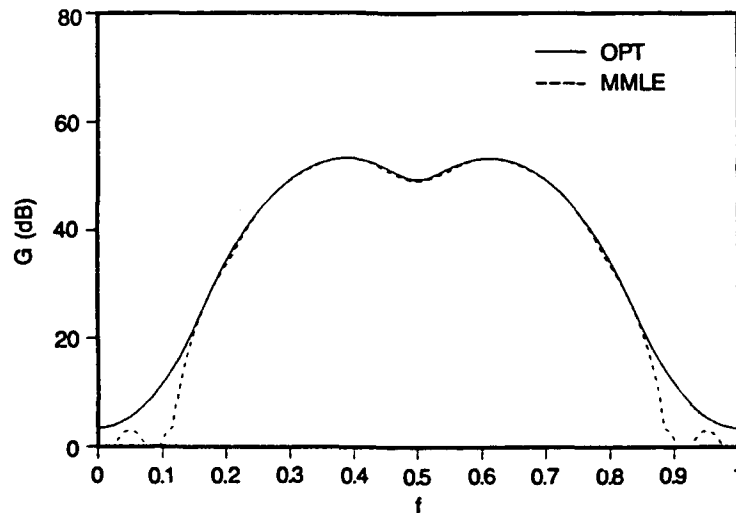


Fig. 15(b) — G vs f , $N = 8$, P_4 , $C/N_0 = 50$ dB, $\sigma T = 0.05$

The MMLE design described above can also be incorporated, and Fig. 16 shows the results for the maximum gains for no missing pulse and for the fourth pulse missing by using an eight-filter MMLE design that uses the same subbands as in Andrews' design. These filters yield a response that is very nearly optimum. However, when the MMLE design procedure [5] is used and subband partitioning is not constrained to that of Andrews, the number of filters can be reduced without a large degradation in performance away from the edges of the band. This is shown in Fig. 17(a) for $N = 8$ when using only three MMLE filters for the no-missing-pulse case and in Fig. 17(b) for $N = 8$ when using three filters for the missing-pulse case.

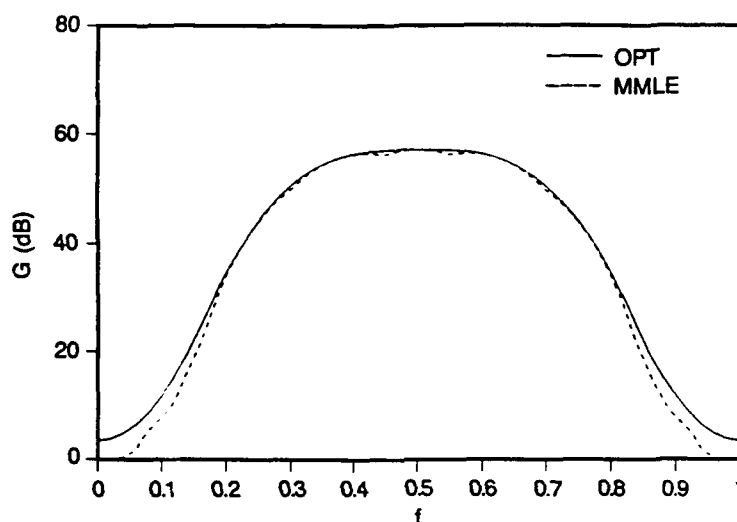


Fig. 16(a) — G vs f , $N = 8$, P_0 , $C/N_0 = 50$ dB, $\sigma T = 0.05$

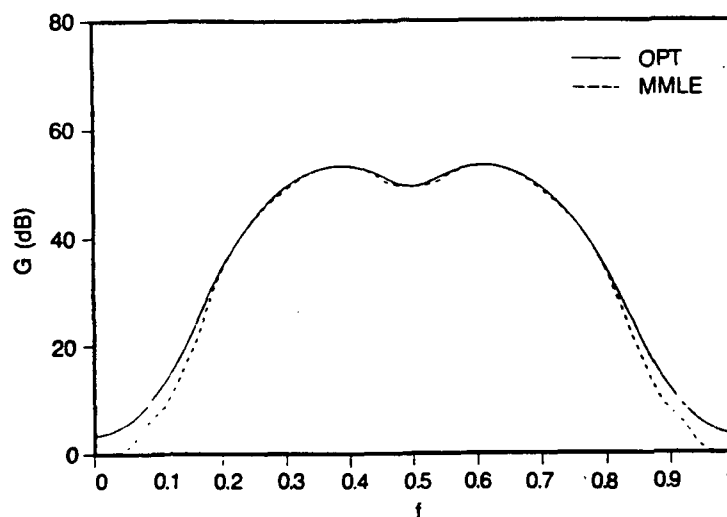
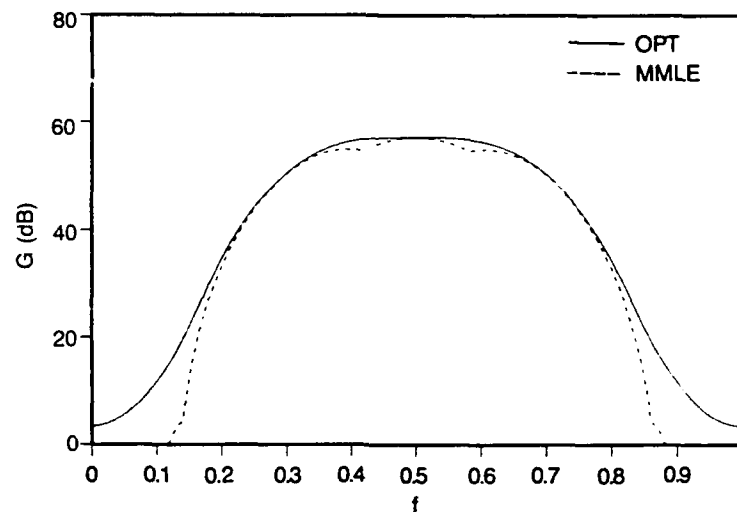
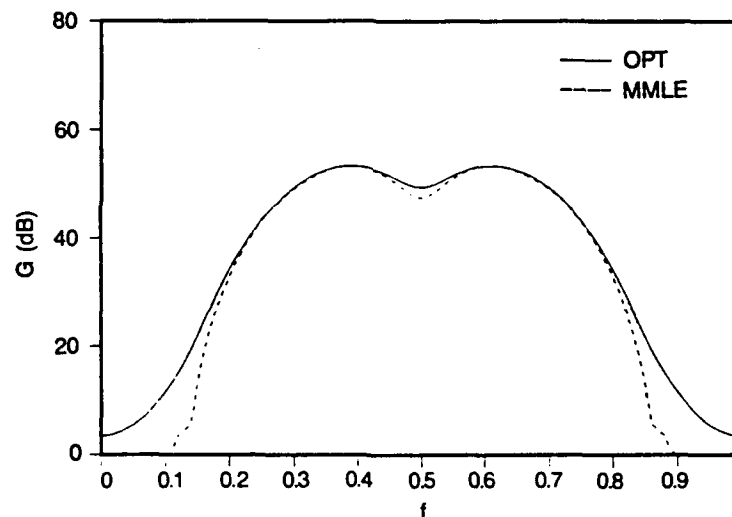


Fig. 16(b) — G vs f , $N = 8$, P_4 , $C/N_0 = 50$ dB, $\sigma T = 0.05$

Fig. 17(a) — G vs f , $N = 8$, P_0 , $C/N_0 = 50$ dB, $\sigma T = 0.05$ Fig. 17(b) — G vs f , $N = 8$, P_4 , $C/N_0 = 50$ dB, $\sigma T = 0.05$

5. IMPLEMENTATION

Figure 18 shows an adaptive implementation for the interference-pulse case. Here the I/Q data enter a radio-frequency interference (RFI) detector. The detector determines if any pulses have been contaminated by strong interference. If so, this information is sent to the blanking circuitry that zeros the value. This information is also sent to a coefficient prom and associated logic that chooses the optimum filter coefficients to be used in the finite impulse response (FIR) filter. This system has the advantage that a separate FIR filter is not needed for every missing-pulse location.

Filter designs such as the MMLE rely heavily on the a priori knowledge of C/N_0 and σT . When these values are not known exactly, these designs may not yield a nearly optimal processor. The issue of robust processor design is a subject of future research.

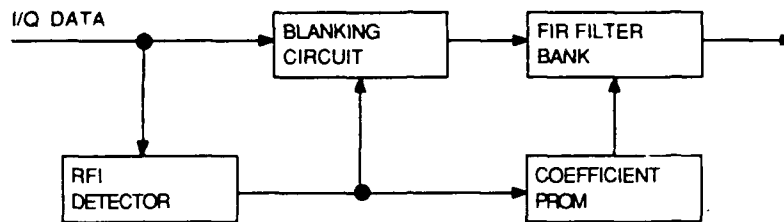


Fig. 18 — Adaptive implementation

6. SUMMARY

In this report we have investigated the degradations incurred with a conventionally weighted MTI or Doppler filter radar when one of the return pulses is missing. This can occur in several different situations: whenever an impulsive interference pulse is blanked, when a return pulse is eclipsed by a transmission, and by returns from an ambiguous range interval if no filler pulses are used. It was shown that for conventional MTI and Doppler filter bank processors the loss in performance can be large. The performance when using theoretically optimum filters was described, and losses relative to the no-missing-pulse case were shown. For the single filter, such as an MTI filter, which is generally used for relatively small N , it was shown that the eigenvector methods for determining the weighting can result in large losses. However, the MMLE was shown to give nearly optimum performance.

For multiple filters, the Andrews method of implementing N filter bands for an N -pulse transmitted waveform was described that maximizes the average gain for each subband. In this method, the signal is assumed to be uniformly distributed within each subband, and the covariance matrix used in the design has missing rows and columns accounting for the missing pulse location. This was shown in the examples investigated to provide nearly optimum performance. Using the MMLE method for the same band partitioning also provided nearly optimal performance. However, it was shown that when using the MMLE design procedure the number of filters could be substantially reduced by using a different partitioning of the frequency bands without incurring a large degradation in performance. Being able to use a reduced number of filters with the MMLE technique allows for a more practical implementation. Design of robust filtering that is nearly optimum over a range of C/N_0 and σT values is the subject of future research.

7. REFERENCES

1. E. Fong, A. Walker, and W. Bath, "Moving Target Indication in the Presence of Radio Frequency Interference," in *Proceedings of the IEEE International Radar Conference*, pp. 292-296, 1985.
2. H.R. Ward, "Doppler Processor Rejection of Range Ambiguous Clutter," *IEEE Trans. Aerospace Electron. Syst.* AES-11, 519-522 (1975).
3. R.C. Emerson, "Some Pulse Doppler and MTI Techniques," in *MTI Radar*, D.C. Schleher, ed. (Artech House, 1978).
4. R.H. Fletcher, "Optimum MTI Velocity Response Functions," in *Asilomar Conference on Circuits, Systems and Computers*, 1983.

5. M.J. Steiner, "A Framework for the Detection of a Target of Unknown Velocity," to be published.
6. G.A. Andrews Jr., "Optimization of Radar Doppler Filters to Maximize Moving Target Detection," in *NAECON Record*, pp. 279-283, 1974.